

Nanoscale

Accepted Manuscript



This is an *Accepted Manuscript*, which has been through the Royal Society of Chemistry peer review process and has been accepted for publication.

Accepted Manuscripts are published online shortly after acceptance, before technical editing, formatting and proof reading. Using this free service, authors can make their results available to the community, in citable form, before we publish the edited article. We will replace this *Accepted Manuscript* with the edited and formatted *Advance Article* as soon as it is available.

You can find more information about *Accepted Manuscripts* in the [Information for Authors](#).

Please note that technical editing may introduce minor changes to the text and/or graphics, which may alter content. The journal's standard [Terms & Conditions](#) and the [Ethical guidelines](#) still apply. In no event shall the Royal Society of Chemistry be held responsible for any errors or omissions in this *Accepted Manuscript* or any consequences arising from the use of any information it contains.

Cite this: DOI: 10.1039/c0xx00000x

www.rsc.org/xxxxxx

ARTICLE TYPE

Solution Processed Polydimethylsiloxane/ Gold Nanostar Flexible Substrates for Plasmonic Sensing

Amane Shiohara^a, Judith Langer^a, Lakshminarayana Polavarapu^a, and Luis M Liz-Marzán^{a,b,*}

5 Received (in XXX, XXX) Xth XXXXXXXXX 20XX, Accepted Xth XXXXXXXXX 20XX

DOI: 10.1039/b000000x

Gold nanostars can display tunable optical properties in the visible and near IR, which lead to strong electromagnetic field enhancement at their tips. We report generalized application of gold nanostars for ultrasensitive identification of molecules, based on both localized surface plasmon resonance (LSPR) and surface enhanced Raman scattering (SERS). We address the requirements of plasmonic sensors, related to sufficiently large areas where nanoparticles are uniformly immobilized with high density, as well as mechanical flexibility, which offers additional advantages for real-world applications. Gold nanostar monolayers were thus immobilized on transparent, flexible polydimethylsiloxane substrates, and their refractive index sensitivity and SERS performance were studied. The application of such substrates for LSPR based molecular sensing is demonstrated via detection of a model analyte, mercaptoundecanoic acid. We further demonstrate SERS-based pesticide detection on fruit skin, by simply covering the fruit surface with the flexible plasmonic substrate, at the area where the target molecule is to be detected. The transparency of the substrate allows SERS detection through backside excitation, thereby facilitating practical implementation.

1. Introduction

Plasmonic nanoparticles of metals such as gold or silver possess a great potential for numerous applications due to their unique optical properties.¹⁻³ Excitation of their localized surface plasmon resonance (LSPR) modes leads to large enhancement of local electric fields near the surface of the plasmonic nanoparticles.^{4,5} Ultrasensitive techniques including surface enhanced Raman scattering (SERS) spectroscopy and LSPR sensing have been developed on the basis of this unique phenomenon. LSPR frequency and plasmon field intensity vary depending on several factors such as size and shape of the nanoparticles, as well as refractive index (RI) changes in the surrounding medium,⁶⁻¹² which is the basis of LSPR sensing. On the other hand, SERS detection is based on the amplification of Raman signals of analyte molecules by the enhancement of electric near field when the analyte is located near excited plasmonic nanostructures. It has been recently demonstrated that nanoparticles with sharp tips show higher sensitivity toward RI changes and much larger near field enhancement, as compared to spherical or smoother nanoparticles,¹³⁻¹⁶ thus rendering spiky nanoparticles excellent platforms for optical sensing and SERS. For this reason, fabrication of metallic nanoparticles has seen significant progress toward morphology control and presence of sharp edges or tips, as in nanobipyramids, nanotriangles or nanostars.^{17,18} In this context, several nanostar synthesis methods have been reported, through either seedless or seed-mediated growth.^{8,16,18-25} However, implementation of real-world

applications of these plasmonic nanoparticles is still a challenge. To achieve this purpose, a number of procedures are available to deposit nanoparticles onto a solid substrate such as glass, which can be used in portable sensing devices,²⁶⁻³¹ as alternatives to lithography-based methods,^{5,32-35} which require costly instrumentation and show difficulty for the fabrication of nanostructures with sharp nanoscale features. On the contrary, solution-based fabrication offers fine control over size and shape of the nanoparticles to be deposited on solid substrates. Most of the previous studies focused on the immobilization of plasmonic nanoparticles on rigid substrates such as glass, which has some limitations over flexibility, or paper, which lacks transparency and thus has limited applicability. Thus, substrates featuring bulk size, transparency and flexibility would offer a great advantage over existing rigid substrates in many ways, since they could be wrapped around non-flat surfaces for detection. Examples could be pesticide detection on fruits or detection of drug molecules or explosives from clothes, as well as detection from a liquid flowing through a flexible tube. This is thus the focus of the present study, in which we selected polydimethylsiloxane (PDMS) as a support for gold nanostars and we show successful preparation of macroscale highly sensitive flexible substrates that can be used for both SERS and LSPR sensing. PDMS is a silicon based organic polymer that behaves as an inert, non-toxic, non-flammable and optically transparent elastomer.³⁶⁻³⁸ These unique characteristics render PDMS a popular solid support for plasmonic nanoparticles toward sensing applications. Since PDMS is transparent and the thickness, shape or size of the support can be easily tuned, the Raman analyte can be confined

between the target material and a nanoparticle modified ultrathin PDMS film, so that SERS signals can be measured through backside excitation and Raman scattering collection. Some reports are available on the immobilization of gold nanoparticles on PDMS substrates via solution processes, however these are usually spherical nanoparticles, which in general lead to weak SERS signals. Thus, we aimed at immobilizing anisotropic nanostructures such as nanostars onto PDMS films for efficient SERS and LSPR sensing. Three different morphologies of gold nanostars were produced and deposited on PDMS by a simple method using chemical adsorption. RI and SERS sensitivities for each type of gold nanostars were evaluated using thiolated and dye molecules as Raman reporters. We additionally demonstrate the potential of these substrates for real-life applications, through an example showing LSPR sensing of mercaptoundecanoic acid and SERS detection of a common pesticide on fruit skin.

2. Materials and methods

2.1. Reagents

Milli-Q water was used throughout all experiments. Tetrachloroauric acid tetrahydrate ($\text{HAuCl}_4 \cdot 4\text{H}_2\text{O}$), silver nitrate (AgNO_3), ascorbic acid (AA), sodium dodecylsulfate (SDS), 3-aminopropyltriethoxysilane (APTES), polyvinylpyrrolidone (PVP), mercaptoundecanoic acid (MUA), astra blue (AB), rhodamine 6G (R6G), 4-aminothiophenol (4-ATP), and thiabendazole were purchased from Sigma-Aldrich and used without further purification. SYLGARD184 Silicone Elastomer kit for PDMS fabrication was purchased Dow Corning. All glassware was washed with *aqua regia* before use.

2.2 Synthesis of Au nanostars

Nanostars were prepared by a previously reported seed-mediated method.²⁵ Citrate stabilized nanoparticle seeds were prepared by adding 15 mL of 1% citrate solution to 100 mL of boiling 1mM HAuCl_4 solution under vigorous stirring. After 15 min of boiling the solution was cooled down to room temperature. The solution volume was kept constant while boiling. The seed solution was stored at 4 °C before use for nanostar growth. Nanostars with three different tip sizes (hereafter S1, S2, and S3) were synthesized by varying $[\text{Ag}^+]$ and $[\text{HCl}]$ in the growth solutions. Briefly, 1 mL of the citrate-stabilized seed solution was added to 100 mL of 0.25 mM HAuCl_4 solution with different amounts of HCl (100 μL of 1M HCl for S1 and S2, and 30 μL for S3). Quickly, different amounts of 0.01 M AgNO_3 solution were added to each solution at room temperature (100 μL for S1, 200 μL for S2, 500 μL for S3), together with 500 μL of 0.1 M ascorbic acid. Longer stability of the nanostars could be achieved by addition of SDS solution (100 μL of 0.01 M). The solution was stirred for 30s as the solution color rapidly turned from light pink to bluish or dark grey. The solutions were then centrifuged at 4000 rpm for 90 min at 4 °C and redispersed in 50 mL of ethanol. The nanostar solutions were stored in the dark at 4 °C. Morphological characterization was carried out by transmission

electron microscopy (TEM; JEOL 2010) and Image J software analysis.

2.3. Preparation of Gold Nanostar/PDMS Flexible Substrates

The PDMS elastomers were fabricated by pouring a mixture of Sylgard 184 elastomer and curing agent (w/w=10:1) on a Piranha washed glass slide and heating at 60 °C over night. As prepared PDMS substrates were washed by sonication with ethanol and vertically soaked in 5% APTES solution in ethanol at 40 °C for 4 h. The substrates were then washed again with ethanol by sonication and vertically soaked in the purified nanostar solution in ethanol overnight. The substrates containing nanostars were washed with water and stored in the dark at 4 °C under nitrogen for further use.

2.4. Refractive Index sensitivity measurements

Extinction spectra of the Au nanostar colloidal solution and Au NS/PDMS substrate were measured using a UV-vis spectrophotometer (Agilent 8453). To determine the RI sensitivity in solution, as-prepared nanostars were dispersed in a mixture of water-ethylene glycol solutions by varying the volume fraction of ethylene glycol from 0 to 100% with an increase of 10% in each step. The RI sensitivity of PDMS/AuNS substrates was measured by recording UV-vis spectra of the substrates by immersion in the corresponding water-ethylene glycol solvent mixture. The refractive indices of the mixed solutions were calculated from the volume fractions of the ingredients according to the Lorentz-Lorenz equation. Values of 1.3334 and 1.4318 were used for the refractive indices of pure water and ethylene glycol, respectively. The LSPR peak shifts for the each nanostar sample were plotted as a function of solvent RI and sensitivity was determined as the slope of the corresponding linear fit. Figures of merit (FOM) were calculated by dividing the RI units by the full width at half maximum (FWHM) of the plasmon peaks from the aqueous dispersions of nanostars. For molecular sensing, a strip of Au nanostar/PDMS substrate was fixed on the side wall of a 1cm plastic cuvette and filled with MUA solutions at different concentrations. The extinction spectra were measured by immersion of the strip in the solution of lowest MUA concentration for 4 h and then gradually increasing the concentration to see an LSPR shift. The same strip was used for the all concentrations for consistency.

2.5. SERS measurements

Standard SERS analyte solutions were prepared using stocks of 4-ATP (10^{-2} M), R6G and AB (10^{-3} M) in ethanol, which were further diluted with Milli-Q water to achieve concentrations ranging from 10^{-4} to 10^{-8} M. Thiabendazole is not soluble in water at neutral pH, so a stock solution was prepared at pH=10. The solid SERS samples were prepared by immersing the nanostar functionalized PDMS slides in aqueous solutions of ATP (10^{-6} M) and AB (10^{-7} M) for at least 4 h. After soaking, the

slides were rinsed with Milli-Q water, dried and deposited onto a glass support. For pesticide detection, PDMS films were soaked in aqueous thiabendazole solutions of different concentrations (from 10^{-7} to 10^{-3} M) for 2 h and placed on a glass slide for SERS measurement. For pesticide detection on fruit skin, pieces of apple and orange skin were first soaked in a thiabendazole solution (10^{-5} M), followed by wrapping a PDMS/AuNS film around the skin, with the nanostars facing it. One important note is that, thin PDMS substrates (~ 0.5 mm) are likely to stick onto the fruit surface, so that the nanostars interact with the molecules on the surface to obtain strong SERS signals. Therefore, we prepared thin PDMS substrates using a mould and nanostars attached to it.

The SERS spectra were recorded with an InVia Renishaw Raman spectrometer equipped with two Peltier charge-coupled detectors (CCD) and a Leica confocal microscope. All SERS signals were collected upon laser excitation with a wavelength of 785 nm and exposition time of 10s using a $100\times$ objective with numerical aperture NA= 0.9. The laser power was set to 0.4 mW. For the detection of pesticides on fruit skin, $50\times$ objective was used.

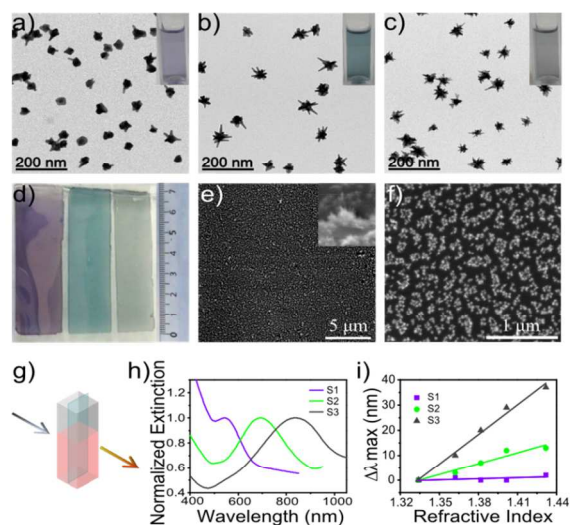


Figure 1: a-c) TEM images of each Au nanostar sample: S1 (a), S2 (b), S3 (c), and photographs of their corresponding solutions. d) Photograph of PDMS slides covered with the nanostars from samples S1, S2 and S3 (Au nanostar/PDMS). e,f) SEM images of Au nanostars (S2)/PDMS at different magnifications. The inset image shows the spikes of Au nanostars deposited on PDMS. g) Schematic image of the configuration for measurement of extinction spectra of PDMS films. h) Extinction spectra of Au nanostars/PDMS substrates immersed in water. i) LSPR shift versus RI for samples of Au nanostars/PDMS substrates. The lines are linear fits to the data.

3. Results and discussion

Au nanostars of three different tip morphologies were prepared by a surfactant free, Ag^+ assisted seed mediated growth method reported by Yuan *et al.*²⁵ (see detailed description in the experimental section). The extinction spectra of the Au nanostars (Figure S1†) clearly show that the tip LSPR mode is highly sensitive on tip morphology. As the concentration of Ag^+ increases, the longitudinal plasmon band red shifts, which is attributed to the average increase of tip length. Figure 1a-c shows representative TEM images of the three different nanostars prepared with varying Ag^+ concentration (10, 20 and 50 μM for samples S1, S2 and S3, respectively) and the corresponding photographs of Au nanostars solutions. The TEM images further confirmed that the number and average length of spikes increases with increasing Ag^+ concentration. The particles in Sample S1 display a small number of tips, so that the UV-vis spectrum is dominated by the core LSPR, while the few longer tips are responsible for a small shoulder around 800 nm.⁸ As the tip aspect ratio increases the main LSPR band gets red-shifted, whereas the extinction spectra of S2 and S3 still show a weak absorption around 520 nm, which is attributed to the (small) contribution of the core LSPR mode (Figure S1†). As the tips exhibit high field enhancement and are highly sensitive to the refractive index of the surrounding medium, they can be very useful for plasmonic sensing. The following step comprised immobilization on flexible supports for the fabrication of flexible plasmonic substrates, for applications where rigid substrates may not be useful. Flexible plasmonic Au nanostars/PDMS substrates were prepared by the attachment of Au nanostars to APTES functionalized-PDMS elastomeric substrates through the amino functional groups. The resulting Au nanostars/PDMS substrates display uniform colorations over areas of several cm^2 , that resemble those of the parent colloidal suspensions, as shown in Figure 1d. The substrates were characterized by UV-vis spectroscopy and SEM. As an example, SEM images of Au nanostars from sample S2 on PDMS are shown in Figure 1e,f. The lower magnification SEM image (Figure 1e) shows a monolayer of nanostars uniformly distributed on the PDMS substrate and sharp tips pointing outwards (see HRSEM image in the inset). The nanostars density was found to be ~ 200 particles per μm^2 . The optical properties and refractive index sensitivity of the three different PDMS/AuNS substrates were characterized by UV-vis spectroscopy through immersion of the substrate in the corresponding solutions in a plastic cuvette, as illustrated in Figure 1g. The extinction spectra of the prepared substrates in water are shown in Figure 1h revealing LSPRs at $\lambda_{\text{max}}(\text{H}_2\text{O})/\text{nm}$ 558, 694, and 835, for substrates S1, S2, and S3 respectively (Table 1). The extinction maximum redshifts upon immobilization of the nanostars on PDMS (immersed in water) with respect to their colloidal suspensions, due to a refractive index increase of the surrounding environment from water to PDMS. Since this type of AuNS are found to be reshape in solution, the stability of PDMS/AuNS substrates was measured under different storage environments. Although some gradual blue shift of the plasmon peak was observed when the substrates

Table 1: Main plasmon peaks, RI sensitivities, FWHM, and FOM of Au nanostars synthesized with different Ag⁺ concentrations, deposited on PDMS films.

	Plasmon Peak (nm)	RIU	FWHM	FOM
Ag 10 μ M	558	14.2	75.35	0.19
Ag 20 μ M	694	116.5	194.14	0.60
Ag 50 μ M	835	392.5	312.65	1.26

were stored in air, when stored under nitrogen no plasmon shift was observed up to 15 days (Figure S2a,b).

Refractive index sensitivity measurements on such flexible PDMS/AuNS substrates were conducted to confirm the performance of the nanostars upon deposition on the substrates. Extinction spectra were measured by immersing the films in water-ethylene glycol solvent mixtures of different volume fractions (Figure 1g). The characterization of the Au nanostars in solution and on PDMS substrates are summarized in Table S1†, Figure S1† and Table 1, respectively, including the LSPR shifts in refractive index units (RIU), as well as figure of merit (FOM). The obtained sensitivities are comparable to those previously reported for Au nanostars,^{6,8} indicating that the tips are indeed available to the solution. The measured RI sensitivities are lower than those previously reported for lithographically fabricated substrates,^{35,39} which is likely due the organic ligand-free nature of these substrates. However, complicated and expensive instrumentation is required in those cases whereas the present solution processing offers advantages in terms of low-cost and easy preparation. We additionally tested the same immobilization approach using other types of Au nanostars, such as those capped with polymers. Therefore, we deposited PVP-coated Au nanostars¹⁶ on PDMS (PDMS/AuNS-PVP) following a similar approach and the data are shown in Figure S3†. This result indicates the general applicability of the method to prepare flexible plasmonic substrates made of different types of anisotropic plasmonic nanostructures. The high sensitivity of Au nanostars with longer tips toward local RI changes suggests potential applications in chemical or biological sensing. We carried out a proof of concept experiment for sensing the adsorption of mercaptoundecanoic acid (MUA), which can covalently adsorb on Au surfaces via thiol binding. MUA can form self-assembled monolayers on gold surfaces and can thus be used as a model system for the LSPR-based molecular sensing. We selected sample S3, which displayed the highest RI sensitivity, to demonstrate MUA molecular sensing. To make sure that the observed plasmon shifts do not originate from morphological differences occurring on the probed nanostars, the PDMS strips were fixed onto the wall of the cuvette, to which

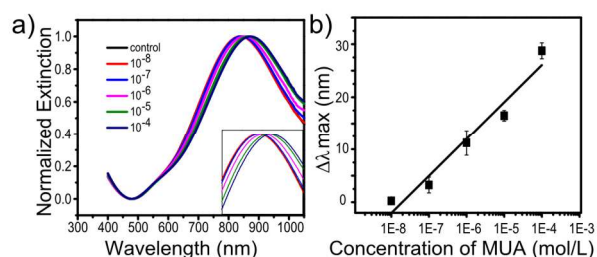


Figure 2: a) Extinction spectra of sample S3 on a PDMS film immersed in different concentrations of MUA in ethanol. b) LSPR shift versus MUA concentration. The solid line is a linear fit to the data.

solutions with increasing MUA concentrations (from 10^{-8} M to 10^{-4} M) were added. The strip was soaked in each solution for 4 hours and then washed with water and ethanol before measuring the corresponding absorption spectrum. Figure 2a shows the slight red shift of the plasmon peak of supported Au nanostars from 840 to 871 nm, when increasing MUA concentration. Interestingly, the shift can be linearly fitted, which is essential for quantitative sensing (see Figure 2b). We found the detection limit at 10^{-7} M and observed the shift up to 10^{-4} M, where saturation of the molecules on the surface of the AuNS was achieved.

Although we demonstrated the potential of PDMS-AuNS substrates in LSPR sensing, application of the same substrates for SERS sensing offers additional advantages, such as very low detection limits, combined with the identification of compounds from their unambiguous vibrational fingerprints, which may ultimately lead to multiplexing. SERS is governed by (i) the electromagnetic field amplification provided by the absorption and scattering behavior of the nanoparticles, which can be tuned by their composition, size and shape, and (ii) the chemical enhancement provided by the coupling of the molecule to the surface, which depends on the electronic nature of the analyte of interest and the relevant surface chemistry. Upon excitation, nanostars show highly localized electromagnetic field (EF) enhancements at the tips, which act as hot spots and thus significantly improve the SERS performance.^{8,40,41} Furthermore, the immobilization of nanostars onto solid supports via aminosilanes gives rise to a uniform assembly containing a high density of inter-particle hot spots with highly confined EF, which may provide even larger SERS than the individual particles.⁴²⁻⁴⁴ To prove the SERS ability and to avoid unrealistically large SERS enhancements caused by resonant Raman scattering of model analytes, we used molecules that are non-resonant with the pump energy of 785 nm, such as the dye astra blue (AB) for electrostatic binding and 4-aminothiophenol (4-ATP) for covalent binding.

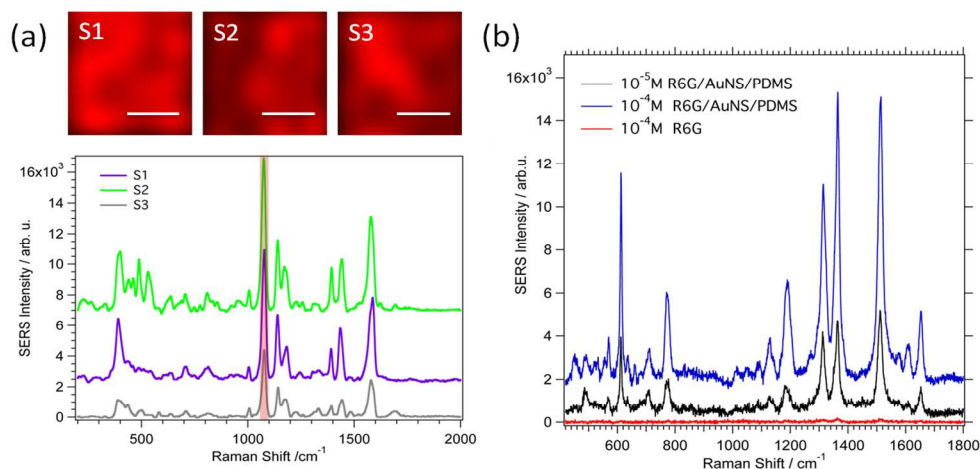


Figure 3: (a) SERS spectra of 4-aminothiophenol [ATP] = 10^{-6} M on nanostars of different aspect ratios: S1 (1.1), S2 (1.7) and S3 (2.4), immobilized onto PDMS. The spectra are background corrected and offsets were applied to improve data presentation. SERS maps over large areas were generated for the characteristic vibrations at 1081 cm^{-1} , corresponding to the $\nu(\text{C-S})$ stretching. The white scale bars on the maps correspond to a scanning distance of $10\text{ }\mu\text{m}$. (b) SERS spectra of 10^{-4} M (blue) and 10^{-5} M (black) R6G solutions drop casted onto a smooth Au surface, covered with PDMS/AuNS films and irradiated from the backside. The Raman scattering spectrum of 10^{-4} M (red) R6G solution onto an Au surface without plasmonic PDMS is shown as a reference. Here, the exposition time and laser power were set to 20s and 0.9 mW, respectively.

PDMS/AuNS slides were cut into ca. $5\times 5\text{ mm}^2$ pieces and incubated in 1 mL of 10^{-7} M AB or 10^{-6} M 4-ATP solutions, prior to SERS measurements. Regardless of the analyte type, the highest SERS efficiency was obtained from sample S2, whereas the trend between S1 and S3 was influenced by the nature of the analyte (see **Figure S4†**). **Figure 3** shows representative spectra and intensity maps for 4-ATP on the three different PDMS/AuNS samples. The characteristic modes observed at 1585, 1179, 1004, 1081 and 397 cm^{-1} , corresponding to ring breathing (8a), ring deformation (9a, 18a), and C-S stretch (7a) and CC torsion (16a) vibrations,⁴⁵⁻⁴⁷ are clearly detectable within all three samples. The intense signals at 1427, 1386 and 1141 cm^{-1} are probably related to laser-induced dimerization of the 4-ATP.⁴⁸ The most efficient SERS performance of S2 is related to the formation of hot spots within the monolayer. It was recently demonstrated at the single particle level that, the number of hot spots as well as the geometry of the cluster strongly increase the SERS enhancement factor under off-resonance conditions in comparison to isolated particles⁴⁴ and strongly increases with decreasing the gap distance between the particles.^{43,49} The SEM image in **Figure 1f** shows a relatively homogeneous distribution of AuNS clusters of different sizes. Probably the combination of medium-sized tip length and symmetric geometry of S2 nanostars lead to tip-to-tip gaps that favor the formation of more active hot spots within the monolayer than for the case of S3 nanostars, which display longer tips that can interlace more easily. Additional factors that may influence the overall SERS intensity are: (i) the number of molecules adsorbed on the nanostars surface and at the hot spots; (ii) the nanoparticle density on the support. As the size of the nanostars increases in the order $S1 < S2 < S3$, the effective concentration of nanostars on the PDMS support (under optimal packing conditions) decreases along the same series and can lead to effectively lower SERS signals.

The homogeneity of the nanostar functionalized PDMS slides was evaluated by measuring SERS spectra over several areas of approx. $20\times 30\text{ }\mu\text{m}^2$. **Figure 3a** shows the SERS intensity distributions for the $\nu(\text{C-S})$ stretching of 4-ATP at 1081 cm^{-1} . In each sample we found a few areas with higher intensities than the average values, leading to brighter spots which are likely due to molecules adsorbed at the tips of the star branches and within the hot spots, thus contributing to a larger extent to the SERS signal.⁴⁰ As SERS is a molecular spectroscopy method, different adsorption sites and orientations with respect to the surface can cause dramatic intensity changes of the excited vibrations. Neglecting these local effects, the mean variation from the average signal does not exceed 10% for all the samples.

The long-term SERS application of the PDMS substrates functionalized with S2 AuNS was furthermore tested for three different batches and aging times using 4-ATP. Concentrations down to 10^{-8} M could be detected even when using 6 and 9 month old substrates. Interestingly, similar PDMS/AuNS substrates could be prepared with PVP-capped nanostars (star tip aspect ratio 1.4), which also showed strong SERS signals with similar intensities than those for surfactant-free nanostars (**Figure S5†**).

From the above SERS studies it is clear that these uniform substrates are suitable candidates for SERS applications. The main advantages of these PDMS supports are the easy preparation, transparency and flexibility. Such substrates can thus be applied to analyze the chemical composition of the surface of objects with arbitrary shapes, by simply wrapping them with a PDMS/AuNS film and exciting the plasmon modes from the rear side of the film. To prove this concept, $10\text{ }\mu\text{L}$ of a dye solution containing rhodamine 6G (R6G) was drop-casted onto a smooth Au film, then covered with a PDMS film functionalized with S2 nanostars and SERS spectra were collected upon backside laser irradiation. As shown in **Figure 3b**, strong SERS signals were recorded (main vibrations at $1515, 1365, 1314$ and 612 cm^{-1}) for

concentrations of 10^{-4} and 10^{-5} M, when R6G was in contact with the plasmonic substrate. In the absence of nanostars, Raman scattering of 10^{-4} M R6G exposed to the smooth Au was only possible at surface defects.

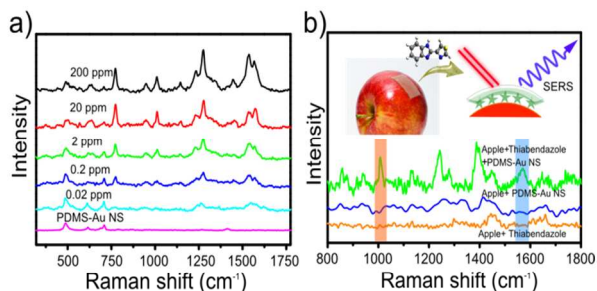


Figure 4. (a) SERS spectra of thiabendazole at various concentrations as indicated, on PDMS/AuNS films, under 785 nm excitation. (b) SERS spectra of thiabendazole adsorbed on apple skin, acquired by wrapping the apple skin with a PDMS/AuNS film and then illuminating from the backside with a 785 nm laser. Control spectra were obtained from apple skin with pesticide but no enhancing substrate and from skin wrapped with Au nanostars/PDMS film but without pesticide. The inset in **b** shows a schematic representation of the detection on apple skin.

After this successful test, the same collection method was applied to detect the pesticide thiabendazole on fruit skin. Thiabendazole is widely used as food preservative and additive in many countries, but it is not approved in the EU, Australia and New Zealand, due to its toxicity at higher doses. Thus, the detection of such pesticide molecules is important. As shown in **Figure 4a**, the SERS spectra of thiabendazole were readily obtained at different concentrations, with the characteristic Raman peaks at 1008 cm^{-1} (phenyl ring breathing mode), 1276 cm^{-1} (skeletal ring C-N, C=N-N stretch) 1539 cm^{-1} (aromatic C=C stretching) and 1574 cm^{-1} (skeletal ring stretching mode). SERS signals were clearly detectable down to 20 ppb using the PDMS/AuNS substrate. To further investigate the advantages of substrate flexibility, SERS signals from pesticide molecules present on an apple skin were detected by placing the Au nanostars/PDMS film around the fruit, in such a way that nanostars touch the skin directly and thus are in close proximity of pesticide molecules, as shown in the inset of **Figure 4b**. In this case, the peaks at 1008 cm^{-1} (phenyl ring breathing mode), and 1574 cm^{-1} (skeletal ring stretching mode) from the pesticide molecule are clearly observed. However, some spectral shifts were observed with respect to the spectrum obtained from direct incubation of the substrate in pesticide solution, which may arise from chemical binding of pesticide molecules in solution via Au-S bonds, which is not likely to occur for molecules that were adsorbed on apple skin. Control spectra were collected from the fruit skin with pesticide molecule but without the SERS substrate, as well as from non-contaminated fruit skin covered with Au nanostars/PDMS substrate, which confirm that the obtained signals indeed originate from thiabendazole. Importantly, thin PDMS substrates ($\sim 0.5\text{ mm}$) were required so that PDMS could be strongly adhered to the fruit surface and to facilitate adjustment of the laser focus on the fruit skin using the $50\times$ objective. Incidentally, general applicability of the approach was

demonstrated through the detection of the same pesticide molecules from orange skin (**Figure S6†**). In both cases, the presence of pesticide on the fruits could be readily identified, though quantification is still difficult to achieve. Despite of some remaining challenges, this initial study shows the potential of this material, with advantages regarding large scale fabrication of flexible plasmonic substrates for sensing of arbitrary analytes on substrates of any shape and composition.

4. Conclusions

Gold nanostars were immobilized onto flexible PDMS substrates via a simple solution process based on electrostatic self-assembly. The refractive index sensitivity of such PDMS-supported Au nanostars allowed LSPR sensing of model molecules such as MUA, showing a linear increase of the LSPR shift with respect to the concentration of MUA. These substrates additionally exhibit high SERS activity toward both thiolated and non-thiolated molecules. The efficiency with regard to the two different sensing methods appears to be optimal for nanostars with different geometries, which may also be related to the formation of clusters on the substrate. Therefore, it is possible to design flexible plasmonic substrates with specific optical properties depending on the sensing method. The flexibility of PDMS offers additional advantages for sensing on substrates with arbitrary geometries, which was demonstrated through the detection of a selected pesticide on fruit skin using back side illumination. Considering the low cost and simple fabrication of the flexible plasmonic substrates using gold nanostars with tunable plasmon resonances, these substrates offer a great potential toward both LSPR and SERS sensing applications. Moreover we expect that these substrates can be readily incorporated into PDMS-based microfluidic devices for online plasmonic sensing.

Notes and references

^a *Bionanoplasmonics Laboratory, CIC biomaGUNE, Paseo de Miramón 182, 20009 Donostia-San Sebastian, Spain. Fax: +34 943005301; Tel: +34 943005300; E-mail: lizmarzan@cicbiomagune.es*

^b *Ikerbasque, Basque Foundation for Science, 48011 Bilbao, Spain.*

† Electronic Supplementary Information (ESI) available: [Details on PVP-NS synthesis, additional extinction spectra, RI sensitivity data, control SERS spectra and detection on orange skin]. See DOI: 10.1039/b000000x/

1. S. A. Maier, M. L. Brongersma, P. G. Kik, S. Meltzer, A. A. G. Requicha and H. A. Atwater, *Adv. Mater.*, 2001, **13**, 1501-1505.
2. M. Grzelczak, J. Perez-Juste, P. Mulvaney and L. M. Liz-Marzan, *Chem. Soc. Rev.*, 2008, **37**, 1783-1791.
3. R. Alvarez-Puebla, L. M. Liz-Marzán and F. J. García de Abajo, *J. Phys. Chem. Lett.*, 2010, **1**, 2428-2434.
4. U. Kreibig, M. Vollmer, *Optical Properties of Metal Clusters*, 1995, Springer Ser. Mater. Sci., Vol. 25.
5. M. Duval Malinsky, K. L. Kelly, G. C. Schatz and R. P. Van Duyne, *J. Phys. Chem. B*, 2001, **105**, 2343-2350.
6. H. Chen, X. Kou, Z. Yang, W. Ni and J. Wang, *Langmuir*, 2008, **24**, 5233-5237.
7. C. J. DeSantis and S. E. Skrabalak, *Langmuir*, 2012, **28**, 9055-9062.

8. S. Barbosa, A. Agrawal, L. Rodríguez-Lorenzo, I. Pastoriza-Santos, R. A. Alvarez-Puebla, A. Kornowski, H. Weller and L. M. Liz-Marzán, *Langmuir*, 2010, **26**, 14943-14950.
9. W. Chemnasiri and F. E. Hernandez, *Sens. Actuators, B*, 2012, **173**, 322-328.
10. L. M. Liz-Marzán, *Langmuir*, 2006, **22**, 32-41.
11. P. Mulvaney, *Langmuir*, 1996, **12**, 788-800.
12. C. Noguez, *J. Phys. Chem. C*, 2007, **111**, 3806-3819.
13. H. Chen, L. Shao, K. C. Woo, T. Ming, H.-Q. Lin and J. Wang, *J. Phys. Chem. C*, 2009, **113**, 17691-17697.
14. E. Hao, R. C. Bailey, G. C. Schatz, J. T. Hupp and S. Li, *Nano Lett.*, 2004, **4**, 327-330.
15. F. Hao, C. L. Nehl, J. H. Hafner and P. Nordlander, *Nano Lett.*, 2007, **7**, 729-732.
16. P. S. Kumar, I. Pastoriza-Santos, B. Rodríguez-González, F. J. G. d. Abajo and L. M. Liz-Marzán, *Nanotechnology*, 2008, **19**, 015606.
17. M. R. Langille, M. L. Personick, J. Zhang and C. A. Mirkin, *J. Am. Chem. Soc.*, 2012, **134**, 14542-14554.
18. J. R. G. Navarro, D. Manchon, F. Lerouge, N. P. Blanchard, S. Marotte, Y. Leverrier, J. Marvel, F. Chaput, G. Micouin, A.-M. Gabudean, A. Mosset, E. Cottancin, P. L. Baldeck, K. Kamada, S. Parola, *Nanotechnology*, 2012, **23**, 465602.
19. P. Pallavicini, A. Doña, A. Casu, G. Chirico, M. Collini, G. Dacarro, A. Falqui, C. Milanese, L. Sironi, A. Taglietti, *Chem. Commun.*, 2013, **49**, 6265-6267.
20. J. Xie, J. Y. Lee and D. I. C. Wang, *Chem. Mater.*, 2007, **19**, 2823-2830.
21. A. Kedia and P. S. Kumar, *J. Mater. Chem. C*, 2013, **1**, 4540-4549.
22. A. Kedia and P. S. Kumar, *Journal of Materials Chemistry C*, 2013, **1**, 4540-4549.
23. S. Umadevi, H. C. Lee, V. Ganesh, X. Feng and T. Hegmann, *Liq. Cryst.*, 2014, **41**, 265-276.
24. W. Moukarzel, J. Fitremann and J.-D. Marty, *Nanoscale*, 2011, **3**, 3285-3290.
25. H. Yuan, C. G. Khoury, H. Hwang, C. M. Wilson, G. A. Grant and T. Vo-Dinh, *Nanotechnology*, 2012, **23**, 075102.
26. Q. Su, X. Ma, J. Dong, C. Jiang and W. Qian, *ACS Appl. Mater. Interfaces*, 2011, **3**, 1873-1879.
27. P. Dong, Y. Lin, J. Deng and J. Di, *ACS Appl. Mater. Interfaces*, 2013, **5**, 2392-2399.
28. Y. Hu, Y. Song, Y. Wang and J. Di, *Thin Solid Films*, 2011, **519**, 6605-6609.
29. S. Vial, I. Pastoriza-Santos, J. Pérez-Juste and L. M. Liz-Marzán, *Langmuir*, 2007, **23**, 4606-4611.
30. S. Abalde-Cela, S. Ho, B. Rodríguez-González, M. A. Correa-Duarte, R. A. Álvarez-Puebla, L. M. Liz-Marzán and N. A. Kotov, *Angew. Chem. Int. Ed.*, 2009, **48**, 5326-5329.
31. M. N. Martin, J. I. Basham, P. Chando and S.-K. Eah, *Langmuir*, 2010, **26**, 7410-7417.
32. M. Fleischer, D. Zhang, K. Braun, S. Jäger, R. Ehlich, M. Häffner, C. Stanciu, J. K. H. Hörber, A. J. Meixner and D. P. Kern, *Nanotechnology*, 2010, **21**, 065301.
33. X. Xu, B. Peng, D. Li, J. Zhang, L. M. Wong, Q. Zhang, S. Wang and Q. Xiong, *Nano Lett.*, 2011, **11**, 3232-3238.
34. M. A. Mahmoud and M. A. El-Sayed, *J. Phys. Chem. B*, 2012, **117**, 4468-4477.
35. O. Vazquez-Mena, T. Sannomiya, M. Tosun, L. G. Villanueva, V. Savu, J. Voros and J. Brugger, *ACS Nano*, 2012, **6**, 5474-5481.
36. L. Polavarapu and L. M. Liz-Marzán, *Phys. Chem. Chem. Phys.*, 2013, **15**, 5288-5300.
37. G. Lu, H. Li and H. Zhang, *Small*, 2012, **8**, 1336-1340.
38. G. Lu, H. Li and H. Zhang, *Chem. Commun.*, 2011, **47**, 8560-8562.
39. K.-L. Lee, P.-W. Chen, S.-H. Wu, J.-B. Huang, S.-Y. Yang and P.-K. Wei, *ACS Nano*, 2012, **6**, 2931-2939.
40. C. G. Khoury and T. Vo-Dinh, *J. Phys. Chem. C*, 2008, **112**, 18849-18859.
41. H. Yuan, Y. Liu, A. M. Fales, Y. L. Li, J. Liu and T. Vo-Dinh, *Anal. Chem.*, 2012, **85**, 208-212.
42. G. Schatz, M. Young and R. Duyne, in *Surface-Enhanced Raman Scattering*, eds. K. Kneipp, M. Moskovits and H. Kneipp, Springer Berlin Heidelberg, 2006, vol. 103, ch. 2, pp. 19-45.
43. S. L. Kleinman, R. R. Frontiera, A.-I. Henry, J. A. Dieringer and R. P. Van Duyne, *Phys. Chem. Chem. Phys.*, 2013, **15**, 21-36.
44. N. Pazos-Perez, C. S. Wagner, J. M. Romo-Herrera, L. M. Liz-Marzán, F. J. García de Abajo, A. Wittemann, A. Fery and R. A. Alvarez-Puebla, *Angew. Chem. Int. Ed.*, 2012, **51**, 12688-12693.
45. K. W. Kho, U. S. Dinis, A. Kumar and M. Olivo, *ACS Nano*, 2012, **6**, 4892-4902.
46. S. Hong, D. Lee, H. Zhang, J. Q. Zhang, J. N. Resvick, A. Khademhosseini, M. R. King, R. Langer and J. M. Karp, *Langmuir*, 2007, **23**, 12261-12268.
47. M. Osawa, N. Matsuda, K. Yoshii and I. Uchida, *J. Phys. Chem.*, 1994, **98**, 12702-12707.
48. Y.-F. Huang, H.-P. Zhu, G.-K. Liu, D.-Y. Wu, B. Ren and Z.-Q. Tian, *J. Am. Chem. Soc.*, 2010, **132**, 9244-9246.
49. K. L. Wustholz, A.-I. Henry, J. M. McMahon, R. G. Freeman, N. Valley, M. E. Piotti, M. J. Natan, G. C. Schatz and R. P. V. Duyne, *J. Am. Chem. Soc.*, 2010, **132**, 10903-10910.

Table of Contents entry:

Au nanostar/PDMS flexible substrates were applied for SERS-based detection of pesticide molecules on fruit skin.

